Hydrol. Earth Syst. Sci. Discuss., https://doi.org/10.5194/hess-2018-466
Manuscript under review for journal Hydrol. Earth Syst. Sci.
Discussion started: 8 October 2018

Hydrology and Earth System Sciences
Discussions

Implementation of salt-induced freezing point depression function into CoupModel_v5 for improvement of modelling seasonally frozen soils

Mousong Wu[1,2,3], Per-Erik Jansson[2], Jingwei Wu[1*], Xiao Tan[1,4], Kang Wang[1], Peng Chen[5], Jiesheng Huang[1]

1. *State Key Laboratory of Water Resources and Hydropower Engineering Science, Wuhan University, 430072 Wuhan, Hubei, China*
2. *Department of Sustainable Development, Environmental Science and Engineering, KTH Royal Institute of Technology, 10044 Stockholm, Sweden*
3. *Department of Physical Geography and Ecosystem Science, Lund University, 23362 Lund, Sweden*
4. *State Key Laboratory of Hydraulics and Mountain River Engineering, College of Water Resource & Hydropower, Sichuan University, 610065 Chengdu, Sichuan, China*
5. *Department of Geology, Lund University, 23362 Lund, Sweden*

Abstract

Soil freezing/thawing is important for soil hydrology and water management in cold regions. Salt in agricultural field impacts soil freezing/thawing characteristics and therefore soil hydrologic process. In this context, we conducted field experiments on soil water, heat and salt dynamics in two seasonally frozen agricultural regions of northern China to understand influences of salt on cold regions hydrology. We developed CoupModel by implementing impacts of salt on freezing point depression. We employed a Monte-Carlo sampling method to calibrate the new model with field observations. The new model improved soil temperature mean error (ME) by 16% to 77% when new freezing point equations were implemented into CoupModel. Nevertheless, we found that parameters related to energy balance and soil freezing characteristics in the new model were sensitive to soil heat and water transport at both sites.

*Correspondence author.
Email: jingwei.wu@whu.edu.cn

Hydrol. Earth Syst. Sci. Discuss., https://doi.org/10.5194/hess-2018-466
Manuscript under review for journal Hydrol. Earth Syst. Sci.
Discussion started: 8 October 2018

However, a systematic model sensitivity and calibration has shown to be able to improve model performance, with mean values of R^2 from behavioral simulations for soil temperature at 5 cm depth as high as 0.87 and 0.90, and mean value of R^2 for simulated soil water (liquid or total water contents at 5 cm depth) of 0.31 and 0.80 at site Qianguo and site Yonglian, respectively. This study provided a new approach considering influences of salt on soil freezing/thawing in numerical models and highlighted the importance of salt in soil hydrology of seasonally frozen agricultural soils.

Keywords: Saline soil; freezing point; seasonal frost; sensitivity; soil hydrology

1. Introduction

Soil freezing and thawing processes have long been recognized for its importance in not only engineering applications (e.g., construction of roads and pipelines) (Jones, 1981; Hansson et al., 2004; Wettlaufer and Worster, 2006), but also environmental issues (e.g., soil erosion, flooding, and pollutants migration) (Andersland et al., 1996; Seyfried and Murdock, 1997; Baker and Spaans, 1997 ; McCauley et al., 2002). Knowledge on soil freezing and thawing could uncover mechanisms on water and salt distribution in soil (Baker and Osterkamp, 1989), on frost heaving (Wettlaufer and Worster, 2006), on waste disposal technology (McCauley et al., 2002), as well as on climate change and water management in cold regions (Lopez et al., 2007).

Laboratory and field experiments on hydrological characteristics of freezing/thawing soils have been conducted to understand soil hydrology in cold regions. Most of the experiments focused on soil freezing characteristics under various climate and soil conditions (Williams, 1964; Black and Tice, 1989; Spaans and Baker, 1996; Azmatch et al., 2012), regional water and energy balance in winter (Fuchs et al., 1978; Baker and Spaans, 1997; Hayashi et al., 2004; Watanabe et al., 2013; Zhou et al., 2014). There were very few studies on salt transport in frozen soils, except for frost heaving. Cary et al. (1979) found salt can decrease frost heaving and increase infiltration in frozen soils based on observations. Konrad and McCammon (1990) found the expulsion of salt from ice is dependent on freezing rate of soil.

Hydrological effects of salt in cold regions have not been deeply explored. Wang et al. (2016) compared water and salt fluxes in two agricultural fields same as in this study, and detected different flow characteristics of salt during soil freezing and thawing seasons. They demonstrated that salt expulsion and dispersion are not negligible in frozen soils. Wu et al. (2016a) found that evaporation during winter was controlled by soil salt and groundwater in field frost tube experiments, in Inner Mongolia, China. They also demonstrated that water, heat and salt transport in frozen soils were coupled, and due to spatial heterogeneity of soil properties and technical difficulties in soil freezing/thawing experiments, measurements contained large uncertainties.

Numerical models on soil freezing/thawing have been put forward by many. Jansson and Karlberg (2004) developed a coupled process-based model—CoupModel, to simulate water, heat as well as salt transport in frozen soil. CoupModel is a process-based model with detailed descriptions on coupled water and heat transport in frozen and unfrozen soils. It has shown to be one of the most robust models among other models taking soil freezing/thawing into account (e.g., SWAP, DRAINMOD, SWAT, HBV, VIC, and ATS etc). This model was developed and applied to forests (Gustafsson et al., 2004; Wu et al., 2013), agricultural field (Wu et al., 2011), permafrost (Zhang et al., 2012; Scherler et al., 2013) and other ecosystems (Okkonen and Kløve, 2011; Khoshkhoo et al., 2015).

However, there were large uncertainties in modeling soil freezing and thawing due to the complexity of phase change and coupled processes. To reduce uncertainties in modeling, uncertainty analysis method was always introduced by combining experimental data with numerical models in calibration of the models for better representativeness of reality. The generalized likelihood uncertainty estimation (GLUE) technique (Beven and Binley, 1992) is the commonly used method for uncertainty analysis in environmental modeling. Instead of searching for an optimal parameter set, the GLUE method generates ensembles of parameter sets that show equally good performance in simulations, called ‘equifinality’ by Beven (2006). GLUE was performed by randomly sampling the parameter space within their ranges using

Hydrol. Earth Syst. Sci. Discuss., https://doi.org/10.5194/hess-2018-466
Manuscript under review for journal Hydrol. Earth Syst. Sci.
Discussion started: 8 October 2018

Monte-Carlo sampling method, and then by selecting behavioral simulations using criteria applied to performance metrics.

In this study, we performed experiments on water, heat and salt transport at two seasonal frost sites located in northern part of China. They are different in climate and in soil conditions, but are both important agricultural regions in northern part of China. The Hetao Irrigation District in China is a typical arid agricultural region suffering from soil salinization due to saline water irrigation, extensive evaporation, as well as soil freezing/thawing (Li et al., 2012). The Songyuan Irrigation District is a typical paddy rice grown region in northeastern part of China, suffering from high salinity due to over-development of salinized field into agricultural field (Liu et al., 2001). Soils in both regions go through freezing/thawing during winter and suffer from salinization in spring. These two sites are crucial in water resources management of China under the concept of water-saving agriculture. Wu et al. (2016b) performed calibration on soil water and heat transport based on one plot in the experimental field in Hetao Irrigation District in Inner Mongolia and found that the influences of salt on soil freezing should be taken into account. Wang et al. (2016) conducted field experiments and analyzed water and solutes transport characteristics at these two above-mentioned sites and demonstrated that salt transport in frozen soils is more complicated than in unfrozen soils due to diffusion and solute rejection. Thus, we developed CoupModel by considering impacts of salt on freezing, and applied the new model to the agricultural sites for modeling water, heat and salt in two seasonal frost soils. The main objective was to 1) develop CoupModel by considering effects of salt on freezing point; 2) identify sensitivity of parameters; 3) analyze uncertainty in modeling soil hydrology in seasonal frost agricultural soils.

2. Material and Methods

2.1 Study sites

Experiments were conducted at two agricultural sites of northern China. One site is located in Qianguo Irrigation District of Songyuan, Jilin province, China (lat: 45.24°, lon: 124.60°, hereafter referred as site

Hydrol. Earth Syst. Sci. Discuss., https://doi.org/10.5194/hess-2018-466
Manuscript under review for journal Hydrol. Earth Syst. Sci.
Discussion started: 8 October 2018

95 Qianguo) (**Fig. 1**). Field experiment at site Qianguo was conducted during 2011/2012 winter. Annual
96 precipitation at site Qianguo is 451 mm and annual mean air temperature is 5.1 ^{o}C (averaged from 2011 to
97 2012). This study site is typical for its soil texture classified as clay, which has a high bulk density, low
98 porosity, and low hydraulic conductivity (**Table 1**). Soil profile at site Qianguo is homogeneous, with
99 porosity of 0.46 and bulk density of 1.42 g cm^{-3}. The water table in this area fluctuates between 1.5 and
100 2.0 m. Maximum frost depth at site Qianguo is 1.2 m. Six plots (2×2 m^2 for each) were selected in a
101 paddy field, which was cultivated with paddy rice from May to October. On 2011/10/09, 20 mm NaBr
102 solution containing 6.5 g L^{-1} Br^- was applied to each plot to from the initial profile for Br^-. Before
103 spraying the solution, stubbles were removed from the plots and surface was ploughed to depth of 20 cm.

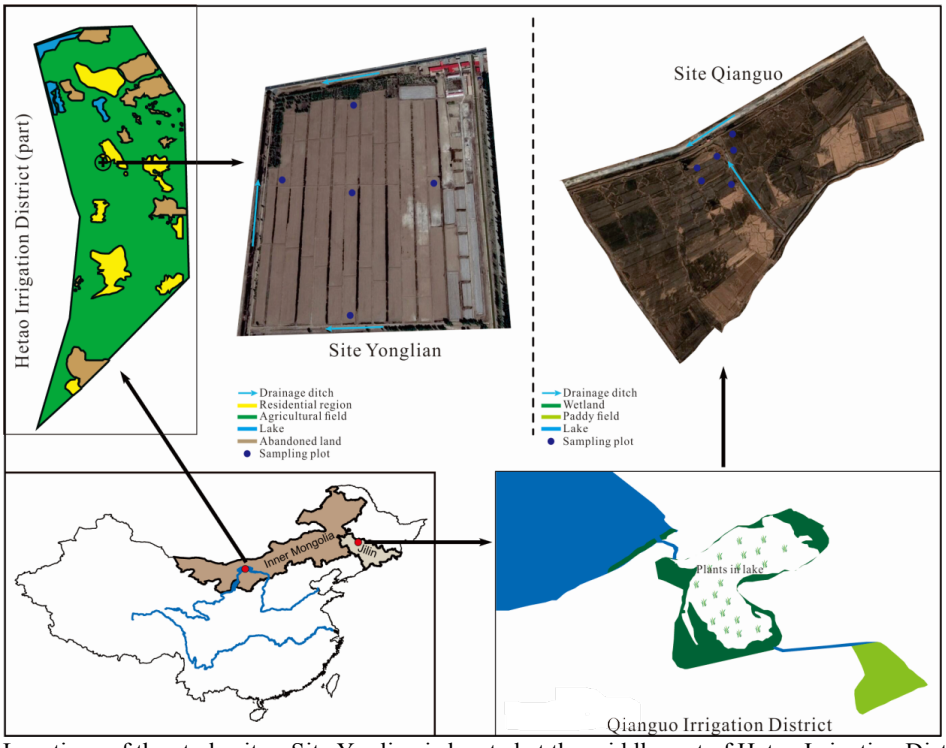

104 **Fig. 1** Locations of the study sites. Site Yonlian is located at the middle part of Hetao Irrigation District of
105 Inner Mongolia Autonomous Region, northern part of China, site Qianguo is located at Songyuan County
106 of Jilin Province, northeastern part of China.

The other site is located at Yonglian experimental station in Hetao Irrigation District of Inner Mongolia Autonomous Region, China (lat: 41.13°, lon: 108.00°, hereafter referred as site Yonglian) (**Fig. 1**). Field experiment at Yonglian was conducted during 2012/2013 winter from October 1st to April 30th. Annual precipitation at this site is 140 mm, and annual mean air temperature is 6.4 °C (averaged for 2012~2013). Soil profile is heterogeneous, with porosity of 0.42-0.46 and bulk density of 1.44-1.53 g cm^{-3} (averaged over 5 plots). Water table fluctuates between 1.5 and 3 m during winter. From November 4th to 6th of 2012, flooding irrigation (autumn irrigation) with 250 mm water was applied to the field for leaching salt that accumulated during growing season. Soil profile mean salt content (mainly NaCl) is 0.1% g g^{-1} for the study site, and irrigation water electrical conductivity is 0.5 mS cm^{-1}. Before autumn irrigation, five plots (2×2 m^2) were selected for experiment at different parts of the agricultural field, and ploughed to 20 cm depth.

Table 1 Soil physical and chemical properties at two study sites Qianguo and Yonglian.

Site	Depth (cm)	Clay (%)	Silt (%)	Sand (%)	Organic matter (%)	Bulk density (g/cm^3)	Porosity (-)
NE	0-140	32.40	38.40	29.30	1.76	1.42	0.46
IM	0-10	27.91	17.20	54.89	0.53	1.49	0.44
	10-20	37.46	21.65	40.90	1.08	1.45	0.45
	20-30	31.69	48.39	19.92	0.77	1.44	0.46
	30-40	34.08	34.32	31.61	0.73	1.45	0.45
	40-60	28.74	34.85	36.40	0.53	1.47	0.45
	60-80	34.67	30.45	34.88	0.77	1.45	0.45
	80-100	17.65	18.46	63.88	1.14	1.53	0.42
	100-140	14.81	35.05	50.15	0.44	1.53	0.42

2.2 Experimental design

Hydrol. Earth Syst. Sci. Discuss., https://doi.org/10.5194/hess-2018-466
Manuscript under review for journal Hydrol. Earth Syst. Sci.
Discussion started: 8 October 2018

TDR probes (Model: CS605, Campell Scientific Inc.) were installed at site Qianguo to detect liquid water content. Due to difficulty in long-term maintaining of TDR system in rural regions, only daily liquid water was manually recorded with a datalogger (TDR 100; Campbell Scientific Inc.). TDR probes were calibrated in laboratory with unfrozen soil, and the precision of calibration was maintained with R^2 of 0.97. TDR probes were then inserted horizontally into the soil pit (10 m apart from the experimental plots) from 5 cm to 100 cm depth with 10 cm interval. PT100 temperature sensors were installed at the same depth as TDR probes, and the daily temperature data were collected.

During soil freezing/thawing season at site Qianguo, 7 sampling dates were chosen (2011/10/09, 2011/11/09, 2011/11/25, 2011/12/20, 2012/02/15, 2012/04/10, 2012/04/20), and soil samples from 0 to 100 cm with 10 cm interval were collected for determining total water content and Br^- content. An electric drill (5 cm in diameter, 10 cm in length) was used for sampling frozen soil for every 10 cm depth. Total water content was determined by oven-dry method. Br^- content was determined by diluting 50 g wet soil into 250 mL deionized water, and measuring the electrical potential (mV) using an electrical potential meter (MP523-06). Then the electrical potential was converted into Br^- concentration by a pre-calibrated relationship between Br^- concentration and electrical potential (calibration R^2=0.99). Soil temperature and liquid water content at 4 depths (5, 15, 25, and 35 cm) from site Qianguo were used to calibrate CoupModel, while soil water storage and salt storage at various depths (0-10 cm, 0-40 cm, 0-100 cm) estimated form soil profile samplings were used to validate the model.

Total water content and Cl^- content from 0 to 100 cm with 10 cm interval at site Yonglian were sampled at 14 dates from October 2012 to April 2013 (2012/10/16, 2012/10/27, 2012/11/10, 2012/12/04, 2012/12/15, 2012/12/26, 2013/01/05, 2013/01/14, 2013/01/25, 2013/03/05, 2013/03/14, 2013/03/25, 2013/04/07, 2013/04/18). The sampling and measurement methods for total water content and Cl^- content were the same as those at site Qianguo. During experimental period (2012/10/01-2013/04/30), hourly soil temperatures at 5, 15, 25 and 35 cm depth were recorded by the PT100 temperature sensors from the micro-meteorological station in the field. Groundwater table depth was measured every day during the

146 autumn irrigation and drainage period (2012/11/4 to 2012/11/15), and for every five days during the rest
147 time of the winter. Soil started freezing from November 12th, 2012, and total thawed on April 30th, 2013.
148 Measuring of groundwater table depth was conducted manually by putting a roped copper cup into
149 observation well, and then measuring the rope length when the cup touched water (by hearing the voice).
150 Soil temperature, soil total water content at 4 depths (5, 15, 25 and 35 cm) and groundwater table depth
151 were used to calibrate CoupModel, while water storage and salt storage at different depths (0-10 cm, 0-40
152 cm, 0-100 cm) estimated from soil profile samplings were used to validate the model.

153 Meteorological data e.g. air temperature, humidity, radiation, wind speed, and precipitation, were
154 obtained from the nearest meteorological station at each site with hourly-resolution from October 1st,
155 2011 to April 30th, 2012 and from October 1st, 2012 to April 30th, 2013 at site Qianguo and site Yonglian,
156 respectively.

157 **3. CoupModel_v5**

158 Model domain covered from soil surface to 6 m depth, with unit area considered. Soil profile was
159 discretized into 16 layers, with 10 cm thickness each layer from 0 to 40 cm, 20 cm thickness from 40 cm
160 to 2 m, and 1 m thickness from 2 m to 6 m. Input meteorological data were hourly, and model time step
161 was set as hourly. Numerical solution of water, heat and salt transport in soils was based on forward
162 difference method. Model performance metrics on different output variables was calculated automatically
163 using modules implemented into CoupModel_v5. Major model processes considered in this study were
164 described in the following sections.

165 *3.1 Soil water processes*

166 CoupModel solved coupled differential equations for water and heat transfer (Jansson, 2012). Water
167 flow in the soil matrix was described by Richards equation:

168 $$\frac{\partial \theta}{\partial t} = \frac{\partial}{\partial z}\left[k_w\left(\frac{\partial \psi}{\partial z} - 1\right)\right] + \frac{\partial}{\partial z}\left(D_v \frac{\partial C_v}{\partial z}\right) - \frac{\partial q_{bypass}}{\partial z} \quad (1)$$

Hydrol. Earth Syst. Sci. Discuss., https://doi.org/10.5194/hess-2018-466
Manuscript under review for journal Hydrol. Earth Syst. Sci.
Discussion started: 8 October 2018

where θ is water content ($m^3\ m^{-3}$); k_w is hydraulic conductivity ($m\ s^{-1}$); ψ is matric potential (m); D_v is vapor diffusion coefficient ($m^2\ s^{-1}$); C_v is vapor density ($m^3\ m^{-3}$); q_{bypass} is the bypass flow in macro pores ($m\ s^{-1}$); z is depth to soil surface (positive downward) (m); and t is time (s).

Vapor flow (second term inside brackets on right side of **Equation (1)**) in soil was determined by vapor gradient between two layers and diffusion coefficient, adjusted by tortuosity d_{vapb} (**Equation (2)**).

$$q_v = d_{vapb} D_0 f_a \frac{\partial C_v}{\partial z} \tag{2}$$

where d_{vapb} is a parameter accounting for tortuosity; D_0 is the diffusion coefficient for free air ($m^2\ s^{-1}$); f_a is the soil air content ($m^3\ m^{-3}$); C_v is vapor density ($m^3\ m^{-3}$); and D_v is vapor diffusion coefficient ($m^2\ s^{-1}$).

The diffusion coefficient for free air, D_0 was a function of soil temperature (**Equation (A1)** in **Table A2**), and vapor density C_v was calculated from vapor pressure (**Equation (A1)**), which was estimated from soil matric potential and soil temperature (**Equation (A1)**).

Infiltration through frozen soil was estimated separately for the low- and high-flow domains (Stähli et al., 1996). CoupModel took the preferential flow in macropores into account using a bypass routine when excess water entering the soil was routed directly to the next underlying soil layer through the high-flow domain (Jansson, 2012). Infiltration into soil was determined by the soil adsorption rate adjusted by a soil matric water adsorption coefficient a_{scale} (**Equation (5)**). When infiltration water was larger than soil adsorption rate, bypass flow would occur. Bypass flow in macro pores was determined by

$$q_{bypass} = \begin{cases} 0 & 1 < q_{in} < s_{mat} \\ q_{in} - q_{mat} & q_{in} \geq s_{mat} \end{cases} \tag{3}$$

$$q_{mat} = \begin{cases} \max\left(k_w(\theta)\left(\frac{\partial \psi}{\partial z} + 1\right), q_{in}\right) & 1 < q_{in} < s_{mat} \\ s_{mat} & q_{in} \geq s_{mat} \end{cases} \tag{4}$$

Hydrol. Earth Syst. Sci. Discuss., https://doi.org/10.5194/hess-2018-466
Manuscript under review for journal Hydrol. Earth Syst. Sci.
Discussion started: 8 October 2018

$$s_{mat} = a_{scale} a_r k_{mat} pF \quad (5)$$

where s_{mat} is soil adsorption rate (m s^{-1}); a_{scale} is soil matric water adsorption coefficient, a_r is a geometry coefficient to describe thickness ratio to horizontal scale of each soil layer; k_{mat} is matric maximum hydraulic conductivity (m s^{-1}); and pF is pF value of soil.

Flow in low-flow domain obeyed Darcy's law and soil water retention curve was determined by Brooks and Corey (1964) equation (**Equation (A3)**), with the air entry at different layers to be adjusted in calibration. Hydraulic conductivity in low-flow domain was calculated from the Mualem (1976) equation (**Equation (A4)**). In frozen soil, hydraulic conductivity was modified for high-flow (Stähli et al., 1996). In high-flow domain, water flow was modeled by gravitational flow under unit gradient, and hydraulic conductivity was adjusted by using impedance factor $c_{\theta,i}$ in high-flow domain (**Equation (6)**):

$$k_{fh} = e^{-\frac{\theta_i}{c_{\theta,i}}} \left(k_w(\theta_{tot}) - k_w\left(\theta_{lf} + \theta_i\right) \right) \quad (6)$$

where $k_w(\theta_{tot})$ is hydraulic conductivity for pores saturated with water (m s^{-1}); $k_w\left(\theta_{lf} + \theta_i\right)$ is hydraulic conductivity when water flow in low domain with ice existence (m s^{-1}); $\theta_i / c_{\theta,i}$ is reduced factor; $c_{\theta,i}$ is impedance factor; θ_{tot} is total water content in high- and low-flow domains (m^3 m^{-3}); θ_{lf} (=$d_1\theta_{wilt}$, **Equation (18)**) and θ_i ($\frac{E-H}{\Delta z L_f \rho_{ice}}$, E is soil heat, J, H is sensible heat, J, L_f is latent heat, J kg^{-1}, Δz is soil thickness, m, ρ_{ice} is ice density, kg m^{-3}) are the liquid water and ice content, respectively, in the low-flow domain (m^3 m^{-3}).

The hydraulic conductivity changed at the freezing front under partially frozen conditions. To prevent excessive water redistribution towards the freezing front, the hydraulic conductivity of partially frozen layers was adjusted by considering ice content influences on water flow using a factor c_{fi} (**Equation (7)**).

$$k_{wf} = 10^{-c_{fi}Q} k_w \quad (7)$$

Hydrol. Earth Syst. Sci. Discuss., https://doi.org/10.5194/hess-2018-466
Manuscript under review for journal Hydrol. Earth Syst. Sci.
Discussion started: 8 October 2018

where c_{fi} is impedance factor; and Q is heat quality, as a ratio of ice content to total water content.

Meanwhile, the influence of soil temperature on soil hydraulic conductivity was considered, using a linear increase factor r_{A1T} and a minimum conductivity k_{minuc} to adjust hydraulic conductivity at 20 °C (**Equation (A7)**).

Surface ponding of water may occur if the soil infiltration capacity was exceeded, otherwise the infiltration rate was equal to precipitation and rates of snowmelt. If infiltration capacity was exceeded, excess water will be transferred to the surface pool. The overland flow from surface pool was estimated by the difference between surface water storage and maximum surface pool, w_{pmax} (**Equation (8)**).

$$q_{\text{surf}} = a_{\text{surf}} \left(W_{\text{pool}} - w_{\text{pmax}} \right) \tag{8}$$

where a_{surf} is an empirical coefficient, W_{pool} is the total amount of water in the surface pool (m), and w_{pmax} is the maximal amount of water stored on soil surface without causing surface runoff (m).

Drainage systems at two study sites were open drainage ditches, drainage at study sites was then calculated by Hooghoudt equation combined with an empirical drainage equation to constitute a manual drainage system, adjusted by initial drainage level z_p and minimum drainage level, drain spacing d_p (**Equation (A9)**), empirical groundwater level peak value z_1, and empirical groundwater flow peak value q_1 (**Equation (A10)**). Meanwhile, initial groundwater level was set for calibration. Groundwater water level was estimated by the soil saturation layer depth to surface.

3.2 Soil heat processes

Heat flow in soil was described by the heat transport equation, considering conduction, convection and latent heat flow:

$$\frac{\partial (CT)}{\partial t} - L_f \rho_i \frac{\partial \theta_i}{\partial t} = \frac{\partial}{\partial z}\left(k_h \frac{\partial T}{\partial t} \right) - C_w \frac{\partial (q_w T)}{\partial z} - L_v \frac{\partial q_v}{\partial z} \tag{9}$$

Hydrol. Earth Syst. Sci. Discuss., https://doi.org/10.5194/hess-2018-466
Manuscript under review for journal Hydrol. Earth Syst. Sci.
Discussion started: 8 October 2018

where C is soil (containing solid, water, and ice) heat capacity (J m^{-3} ^{o}C^{-1}); T is temperature (^{o}C); L_f is latent heat of freezing (J kg^{-1}); ρ_i is density of ice (kg m^{-3}); θ_i is ice content (m^3 m^{-3}); k_h is thermal conductivity soil (W m^{-1} ^{o}C^{-1}); q_w is water flux (m s^{-1}); L_v is latent heat of vaporization (J kg^{-1}); and q_v is vapor flux (m s^{-1}).

Upper boundary for soil heat flow was soil temperature at surface, calculated by the energy balance scheme described in *Section 3.4*. Lower boundary for soil heat flow was controlled by soil temperature fluctuation at 6 m depth, which was estimated using an analytical solution for soil heat conduction.

Soil thermal conductivity for both frozen and unfrozen soils was calculated from the Ballard & Arp equation (Balland and Arp, 2005), adjusted by three empirical coefficients α, β, and a (**Equation (A11)**). Thermal conductivity from the top frozen soil layer was then corrected by using a damping function, adjusted by the maximum damping coefficient C_{md} (**Equation (A12)**). When infiltration water passed the high-flow domain, it would refreeze due to low soil temperature in frozen soils. Meanwhile, latent heat released from refreezing would melt water in high-flow domain. This would lead to redistribution of water between low-flow and high-flow domains. CoupModel considered the water redistribution and adjusted it by a heat transfer coefficient α_h (**Equation (A13)**).

3.3 Salt tracer processes

Salt in CoupModel was simulated as a tracer migrating with water, neglecting diffusion. Salt transport was simulated as Cl$^-$ transport in soil for estimate of salt tracer flux. Salt balance in soil is calculated as:

$$\frac{\partial c_{Cl}}{\partial t} = -\frac{\partial}{\partial z}(q_{mat} c_{Cl}) - \frac{\partial}{\partial z}(q_{bypass} c_{Cldep}) \quad (10)$$

where c_{Cl} is concentration of Cl$^-$ (kg m^{-3}); c_{Cldep} is salt deposition concentration (kg m^{-3}); q_{mat} is water flux (m s^{-1}), q_{bypass} is bypass flow (m s^{-1}).

Hydrol. Earth Syst. Sci. Discuss., https://doi.org/10.5194/hess-2018-466
Manuscript under review for journal Hydrol. Earth Syst. Sci.
Discussion started: 8 October 2018

Soil salt concentration for each layer was then calculated by

$$c_{Cl}(z) = \frac{s_{Cl}(z)(1-s_{adc}(z))}{\theta(z)\Delta z} \quad (11)$$

where s_{Cl} is salt amount at each soil layer (kg m^{-2}); s_{adc} is salt adsorption rate; θ is soil water content at each layer (m^3 m^{-3}); Δz is soil layer thickness (m).

Salt at surface was balanced by salt in precipitation and irrigation, as well as salt loss from surface runoff. Lower and lateral boundaries for salt transport were salt leaching to groundwater, which was proportional to drainage rate. Initial salt concentration c_{Cl}, precipitation salt concentration c_{Cldep}, irrigation salt concentration $c_{Clirrig}$, as well as salt adsorption coefficient s_{adc} at different depths were set as calibration parameters. At site Qianguo, Br^- transport was converted to Cl^- transport in the simulation in the validation of salt storage, Cl^- storage at site Qianguo was then converted to Br^- storage in comparison with field observations of Br^- storage.

3.4 Energy balance processes

Surface temperature and evaporation was calculated using energy balance method, with net short-wave radiation balanced by latent heat, sensible heat and soil heat flux at surface:

$$R_s = L_v E_v + H_s + q_h \quad (12)$$

where L_vE_s is the sum of latent heat flux (J m^{-2} s^{-1}); H_s is sensible heat flux (J m^{-2} s^{-1}) and q_h is heat flux to the soil (J m^{-2} s^{-1}).

Latent heat was calculated as below,

$$L_vE_s = \frac{\rho_a c_p}{\gamma}\frac{(e_{\text{surf}} - e_a)}{r_{as}} \quad (13)$$

Hydrol. Earth Syst. Sci. Discuss., https://doi.org/10.5194/hess-2018-466
Manuscript under review for journal Hydrol. Earth Syst. Sci.
Discussion started: 8 October 2018

where r_{as} is the aerodynamic resistance (m^{-1}); e_{surf} is the vapor pressure at the soil surface (Pa or in m water); e_a is the actual vapor pressure in the air (Pa or in m water); ρ_a is the air density (kg m^{-3}); c_p is the heat capacity of air (J kg^{-1} $^oC^{-1}$); L_v is the latent heat of vaporization (J kg^{-1}) and γ is the psychometric constant.

Sensible heat was calculated as

$$H_s = \rho_a c_p \frac{(T_s - T_a)}{r_{as}} \quad (14)$$

where T_s is the soil surface temperature (^{o}C); T_a is the air temperature (^{o}C); and r_{as}, ρ_a, c_p are the same as **Equation (13)**.

Soil surface heat flow was then calculated,

$$q_h = k_h \frac{(T_s - T_1)}{\frac{\Delta z_1}{2}} + Lq_{v,s} \quad (15)$$

where k_h is the thermal conductivity of the topsoil layer (W m^{-1} $^oC^{-1}$); T_s is the soil surface temperature (^{o}C); T_1 is the middle of uppermost soil compartment temperature (^{o}C); Δz_1 is the depth of the uppermost soil compartment (m) and $Lq_{v,s}$ is the latent water vapor flow from soil surface to the central point of the uppermost soil layer (J m^{-2} s^{-1}).

Surface temperature was then adjusted to make Equation (5) balanced by different fluxes at surface. Soil surface vapor pressure was determined by soil surface temperature, water potential at top layer and soil water gradient between soil surface and top layer. This was further corrected by an empirical factor, which was adjusted by an adjustment coefficient ψ_{eg}, and the surface water balance (**Equation (A14)**), which was adjusted by maximum soil surface water deficit s_{def} and maximum soil surface water excess s_{excess} (**Equation (A15)**).

Hydrol. Earth Syst. Sci. Discuss., https://doi.org/10.5194/hess-2018-466
Manuscript under review for journal Hydrol. Earth Syst. Sci.
Discussion started: 8 October 2018

Aerodynamic resistance for stable atmosphere was calculated using the Richardson equation. Then the aerodynamic resistance for stable atmosphere was adjusted by the momentum roughness length of soil and snow surface z_{0M} ($z_{0M,snow}$) (**Equation (A16)**), and the heat roughness length of surface z_{0H} was derived from z_{0M} and kB^{-1} (**Equation (A17)**). In addition, when surface was at extreme stability conditions, aerodynamic resistance was then adjusted by using a windless exchange coefficient $r_{a,max}^{-1}$ (**Equation (A18)**).

Soil evaporation was adjusted by maximum soil water condensation rate $e_{max,cond}$ considering the influences of condensation of water on evaporation (**Equation (A19)**). Net radiation was estimated by Konzelmann equation with two formulae to calculate longwave radiation and was adjusted by an empirical coefficient r_{k1} (**Equation (A20)**). Snow melting was determined by solving energy balance equation in snowpack using the same scheme as soil surface energy balance calculation. Snow mass balance was then estimated based on temperature change in snowpack as well as snow age. Snow thermal conductivity was calculated from snow density with an adjustment factor s_k (**Equation (A21)**). Soil albedo was determined by albedo of dry and wet soils, adjusted by an empirical coefficient k_a (**Equation (A22)**). Snow albedo was determined by snow age, as well as cumulative air temperature since the latest snowfall, adjusted by the minimum snow albedo a_{min} (**Equation (A23)**).

3.5 Soil freezing point depression function development

To solve the coupled water and heat flow equations, we needed a relation between soil temperature and soil liquid water, i.e. soil freezing characteristics. In frozen soil, when soil temperature was below zero, latent heat changed due to ice formation. When soil temperature continued decreasing, sensible heat also changed. In CoupModel, we assumed that soil is totally frozen when temperature was below T_f (-5 ^{o}C), when soil temperature was between 0 and T_f, sensible heat in soil was calculated as:

$$H = E\left(1 - \frac{L_f(w - \Delta z d_1 \theta_{wilt} \rho_w)}{E_f}\right)(1 - r) \quad (16)$$

Hydrol. Earth Syst. Sci. Discuss., https://doi.org/10.5194/hess-2018-466
Manuscript under review for journal Hydrol. Earth Syst. Sci.
Discussion started: 8 October 2018

where E is total heat stored in soil (J); L_f is latent heat of freezing (J kg^{-1}); w is water stored in soil (kg); Δz is soil thickness (m); d_1 is a factor accounting for the fraction of unfrozen water to soil wilting point water content; θ_{wilt} is the wilting point water content when the pF value of soil water is 4.2 (m^3 m^{-3}); ρ_w is density of water (kg m^{-3}); E_f is energy when soil is totally frozen ($C_f T_f - L_f w_{ice}$, i.e. when soil temperature is T_f, C_f is heat capacity of frozen soil, J kg^{-1} ^{o}C^{-1}); r is freezing point depression.

In modeling of soil frost, when soil was totally frozen at -5 ^{o}C, the liquid water content was determined by wilting point of soil ($\Delta z d_1 \theta_{wilt} \rho_w$), and adjusted by a coefficient d_1, as depicted in **Equation (16)**. Ice content in soil was calculated as:

$$\theta_i = \begin{cases} 0, T > T_0 \\ \frac{E-H}{\Delta z L_f \rho_{ice}}, T_f < T \le T_0 \\ \theta - d_1 \theta_{wilt}, T \le T_f \end{cases} \quad (17)$$

where E is total energy stored in soil (J); H is total energy stored in soil (=$C_f T$, J); L_f is latent heat of freezing (J kg^{-1}); Δz is soil thickness (m); d_1 is a factor accounting for the fraction of unfrozen water to soil wilting point water content; θ_{wilt} is the wilting point water content when the pF value of soil water is 4.2 (m^3 m^{-3}); ρ_{ice} is density of ice (kg m^{-3}).

In CoupModel, the freezing-point depression was related to soil heat storage as below:

$$r = \left(1 - \frac{E}{E_f}\right)^{d_2 \lambda + d_3} \min\left(1, \frac{E_f - E}{E_f + L_f w_{ice}}\right) \quad (18)$$

where d_2, d_3 are empirical constants; λ is the pore size distribution index; w_{ice} is water available for freezing, kg, i.e. ($w - \Delta z d_1 \theta_{wilt} \rho_w$) in **Equation (18)**; E_f is soil heat storage when soil temperature is T_f ($C_f T_f - L_f w_{ice}$), J.

Hydrol. Earth Syst. Sci. Discuss., https://doi.org/10.5194/hess-2018-466
Manuscript under review for journal Hydrol. Earth Syst. Sci.
Discussion started: 8 October 2018

In saline frozen soil, ice formation does not start at 0 °C, but below 0 °C. Freezing point T_0 (**Equation (19)**) is a parameter related to soil type, salt type and salt content. In CoupModel, T_0 was assumed as 0 °C, which was not suitable for saline soils. In this study, two methods were implemented to consider salt influences on freezing point depression. The first one was to set freezing point T_0 as a parameter in the model, and this parameter could be determined by experiments on freezing point of different saline soils. The second method was to relate T_0 to osmotic potential (**Equation (19)**). According to Banin and Anderson (1974), the relationship between freezing point and salt solution could be written as below:

$$T_0 = -10^{-4+sc} \times \frac{\pi}{1.221} \tag{19}$$

where T_0 is the freezing point (°C); π is osmotic potential (in unit cm); sc is a scale factor for considering the influences of salt types on the relationship (range from -2 to 2); -4 is a constant for converting osmotic potential unit from cm to MPa.

Soil salt and soil heat and water transport as well as soil freezing/thawing was connected by **Equation (19)** with osmotic potential π, and freezing point would change as soil temperature and soil salt concentration changed during simulation, since osmotic potential was determined by both soil temperature and salt concentration:

$$\pi(z) = R(T + 273.15)\frac{c_{Cl}(z)}{M_{Cl}} \tag{20}$$

where R is gas constant; T is soil temperature (K); c_{Cl} is salt concentration (kg m^{-3}); M_{Cl} is mole mass of Cl (35.5 g mol^{-1}).

3.6 Calibration approach

The sensitivity analysis and model calibration procedures are summarized in **Fig. 2**. We selected 58 parameters that have either shown a large influence on modeled water and heat dynamics in previous

studies and/or are known to be important in sensitivity analysis (cf. Gustafsson et al., 2001; Wu et al., 2011; Metzger et al., 2015). The 58 parameters represented the major processes related to soil water, heat, radiation as well as salt transport, 19 related to soil water process, 8 related to soil heat process, 19 related to soil salt process, and 12 related to energy balance process (**Table A1**). We noted that 58 parameters made the calibration very inefficient, since some of the parameters were assigned to different layers and some were not so sensitive in comparison with others. We thus conducted a two-step calibration, with the first step to find out the most important parameters from different model processes based on sensitivity analysis, and the second step to calibrate the important parameters.

In the first step, the 58 parameters were tested for each site with 70000 simulations based on Monte Carlo sampling method. Each of the simulations was run with randomly selected parameter values, thus creating 70000 realizations. The most sensitive model parameters were then identified for each site based on their relative importance on performance metrics (e.g. R^2, determination coefficient between simulation and observations, and ME, the mean deviations between simulation and observations). This was done by using the LGM (Lindeman, Gold and Merenda) method (Lindeman et al., 1980) that averages the sequential sums of squares over all orderings of regressors, which calculates the relative importance of each parameter on model performance metrics and ranks them. Based on the ranking of parameters, 8 to 11 sensitive parameters (i.e. 3 common parameters for two sites, another 5 for site Qianguo and another 8 for site Yonglian) were then selected in the second step with 10000 simulations for each site. It is important to note that the sensitive parameters may be different from site to site depending on site-specific characteristics, although initial parameters and their ranges were equivalent for all sites.

Hydrol. Earth Syst. Sci. Discuss., https://doi.org/10.5194/hess-2018-466
Manuscript under review for journal Hydrol. Earth Syst. Sci.
Discussion started: 8 October 2018

Hydrology and Earth System Sciences
Discussions

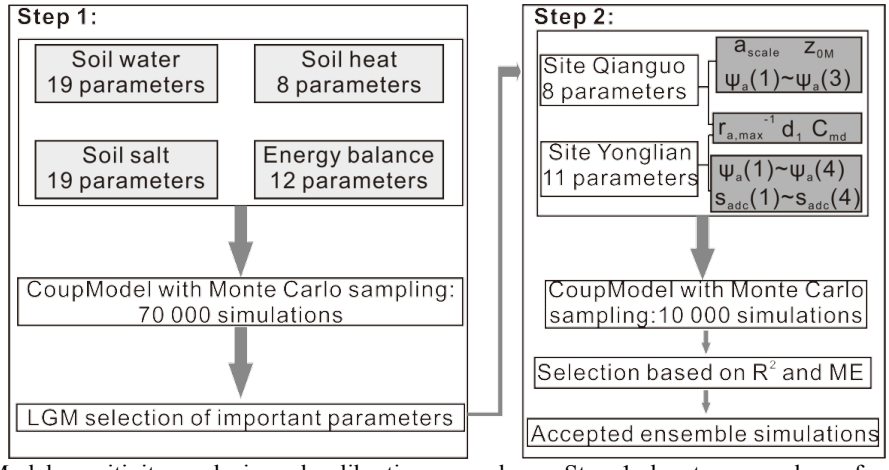

374 **Fig. 2** Model sensitivity analysis and calibration procedures. Step 1 denotes procedures for selecting
375 important parameters with LGM method, step 2 represents model calibration and selection of acceptable
376 simulations.

377 From the 10000 simulations of the second calibration step, ensemble of parameter sets for each site
378 was then selected based on statistical performance metrics (determination coefficient R^2 and mean error
379 ME) for temperature and water at several depths (**Table 2**). In addition to useful information about site-
380 specific processes and their representations in the model, the ensemble simulation results (9 for site
381 Qianguo, 16 for site Yonglian) simulated using accepted parameter sets were used for analysis water,
382 energy and salt balance over the simulation period.

383 **Table 2** Criteria applied to model performance metrics in selection of behavioral simulations.

Site name	Qianguo				Yonglian			
Soil depth	R^2		ME		R^2		ME	
	T	θ	T (°C)	θ (%)	T	θ	T (°C)	θ (%)
5cm	[0.85,1]	[0.3,1]	[-1,1]	[-5,5]	[0.9,1]	[0.5,1]	[-0.5,0.5]	[-3,3]
15 cm	[0.9,1]	[0.8,1]	[-0.5,0.5]	[-5,5]	[0.9,1]	[0.5,1]	[-0.5,0.5]	[-3,3]
25 cm	[0.9,1]	[0.5,1]	[-0.5,0.5]	[-3,3]	[0.9,1]	[0.5,1]	[-0.5,0.5]	[-3,3]
35 cm	[0.85,1]	[0.7,1]	[-0.5,0.5]	[-2,2]	[0.9,1]	[0.5,1]	[-0.5,0.5]	[-3,3]
[a]GWTD	/	/	/	/		[0.6,1]		[b][-0.1,0.1]

384 [a]GWTD is ground water table depth
385 [b]unit for GWTD is m

Hydrol. Earth Syst. Sci. Discuss., https://doi.org/10.5194/hess-2018-466
Manuscript under review for journal Hydrol. Earth Syst. Sci.
Discussion started: 8 October 2018

Hydrology and Earth System Sciences
Discussions

386

387 **4. Results and Discussion**

388 *4.1 Freezing point depression*

389 In **Fig. 3** and **Fig. 4**, the sensitivity of model to freezing point depression is analyzed at 5 cm depth
390 (the same was done for other soil depths, not shown here), based on model results from one of the
391 behavioral simulations at each site. The influences of freezing point on soil heat are obvious (**Fig. 3**).
392 When soil freezing temperature changed from 0 °C to below zero, the relationship between soil
393 temperature and soil heat storage changed accordingly. The model performance was improved when
394 freezing point depression was related to soil salt. Mean error (ME) for soil temperature at 5 cm depth
395 decreased from 1.25 °C to 0.29 °C (improved by 77%) at site Qianguo, and from 2.54 °C to 1.83 °C
396 (improved by 28%) at site Yonglian, when freezing point decreased from 0 °C to -3 °C.

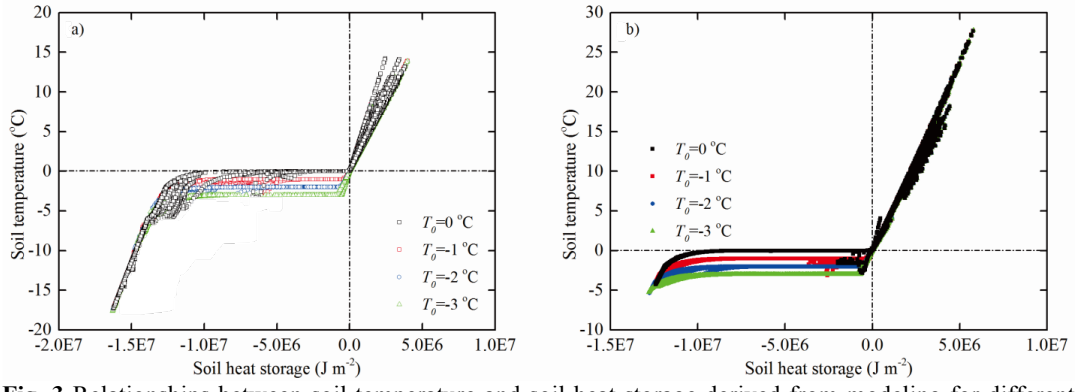

397 **Fig. 3** Relationships between soil temperature and soil heat storage derived from modeling for different
398 freezing points at 5 cm depth at a) site Qianguo and b) site Yonglian.

399 The relationships between soil temperature and soil heat storage at 5 cm depth were different when
400 various *sc* values were assigned (**Fig. 4**). This indicated that different types of salt also influence soil
401 freezing/thawing. Meanwhile, ME decreased from 1.35 °C to 0.64 °C (improved by 53%) when *sc*
402 changed from 0 to 1 at site Qianguo. At site Yonglian, ME decreased from 2.54 °C when *sc* is 0 to 2.14

Hydrol. Earth Syst. Sci. Discuss., https://doi.org/10.5194/hess-2018-466
Manuscript under review for journal Hydrol. Earth Syst. Sci.
Discussion started: 8 October 2018

403 °C (improved by 16%) when sc was 1. This indicated that in determination of freezing point, not only the
404 salt content, but also the salt type should be taken into consideration for reducing uncertainty in modeling
405 soil temperature.

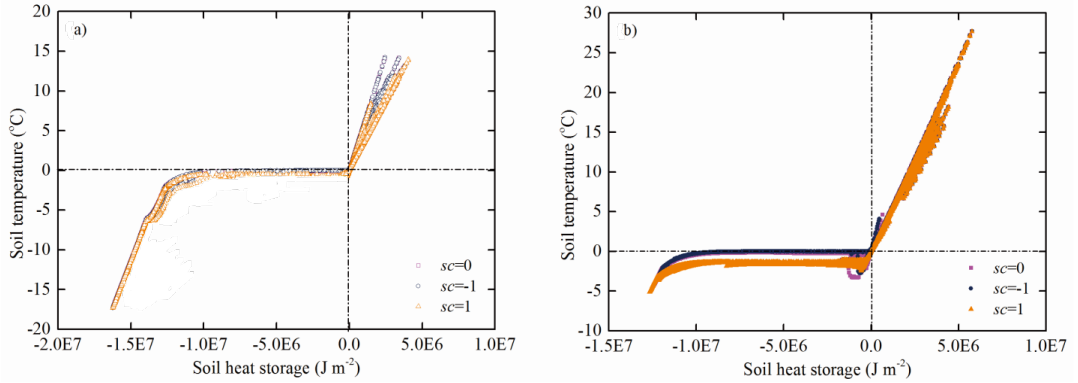

406 **Fig. 4** Relationships between soil temperature and soil heat storage derived from modeling for different *sc*
407 values at 5 cm depth at a) site Qianguo and b) site Yonglian.

408 *4.2 LGM relative importance in calibration parameters*

409 At site Qianguo, for soil temperature R^2 at 4 depths (**Fig. 5** a)-d)), $z_{oM,snow}$ (momentum roughness
410 length of snow), which is to estimate surface aerodynamic resistance, was found to be most important.
411 This parameter would influence surface energy balance and eventually impact heat transport in soil
412 profile. The other important parameter for soil temperature R^2 at 15, 25 and 35 cm depths was C_{md}, which
413 is a parameter to adjust thermal conductivity of surface frozen layer.

414 For liquid water content R^2 at 4 depths (**Fig. 5** e)-h)), the most important parameters were $z_{0M,snow}$,
415 $r_{a,max}^{-1}$, d_1 and ψ_a of different depths that were related to energy balance and soil heat and water transport.
416 $z_{0M,snow}$ was already detected to be important for soil temperature. This indicated that surface energy
417 balance in snowpack at site Qianguo is important for both soil heat and water transport.

418

Hydrol. Earth Syst. Sci. Discuss., https://doi.org/10.5194/hess-2018-466
Manuscript under review for journal Hydrol. Earth Syst. Sci.
Discussion started: 8 October 2018

Hydrology and Earth System Sciences
Discussions
Open Access
EGU

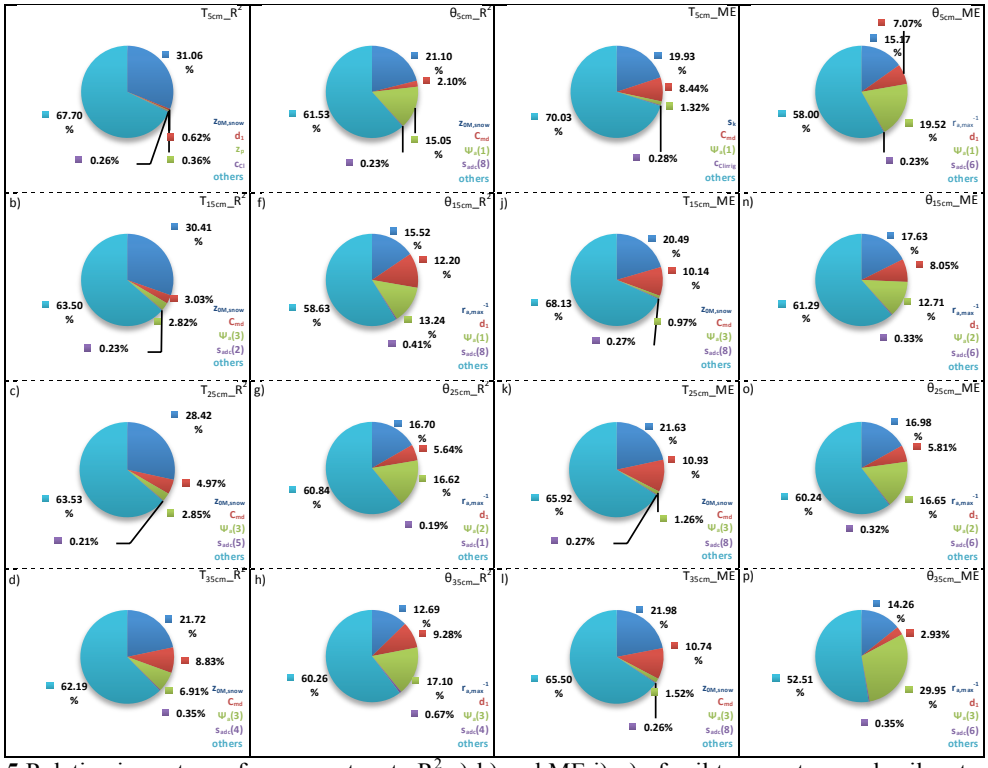

419 **Fig. 5** Relative importance for parameters to R^2 a)-h) and ME i)-p) of soil temperature and soil water at 4
420 depths (5, 15, 25, 35 cm) at site Qianguo. Parameters shown in each sub-figure are the most important
421 parameter from each group, i.e. energy balance, soil heat, soil water, soil salt, and the other parameters.

422 For soil temperature ME at site Qianguo (**Fig. 5** i)-l)), important parameters were similar to soil
423 temperature R^2, except at 5 cm depth, with s_k showing the greatest importance (**Fig. 5** i)). s_k is for
424 estimate of snow thermal conductivity, and determines energy balance in snowpack. Site Qianguo was
425 covered by snow during soil freezing, thus accurate estimates of snow energy balance would help in
426 improving model performance on soil temperature. At site Qianguo, important parameters for soil liquid
427 water content ME were similar to R^2, showing that parameters related to surface energy balance ($r_{a,max}^{-1}$),
428 soil freezing characteristics (d_1) and soil water characteristics (ψ_a) have great importance to soil water
429 transport.

Hydrol. Earth Syst. Sci. Discuss., https://doi.org/10.5194/hess-2018-466
Manuscript under review for journal Hydrol. Earth Syst. Sci.
Discussion started: 8 October 2018

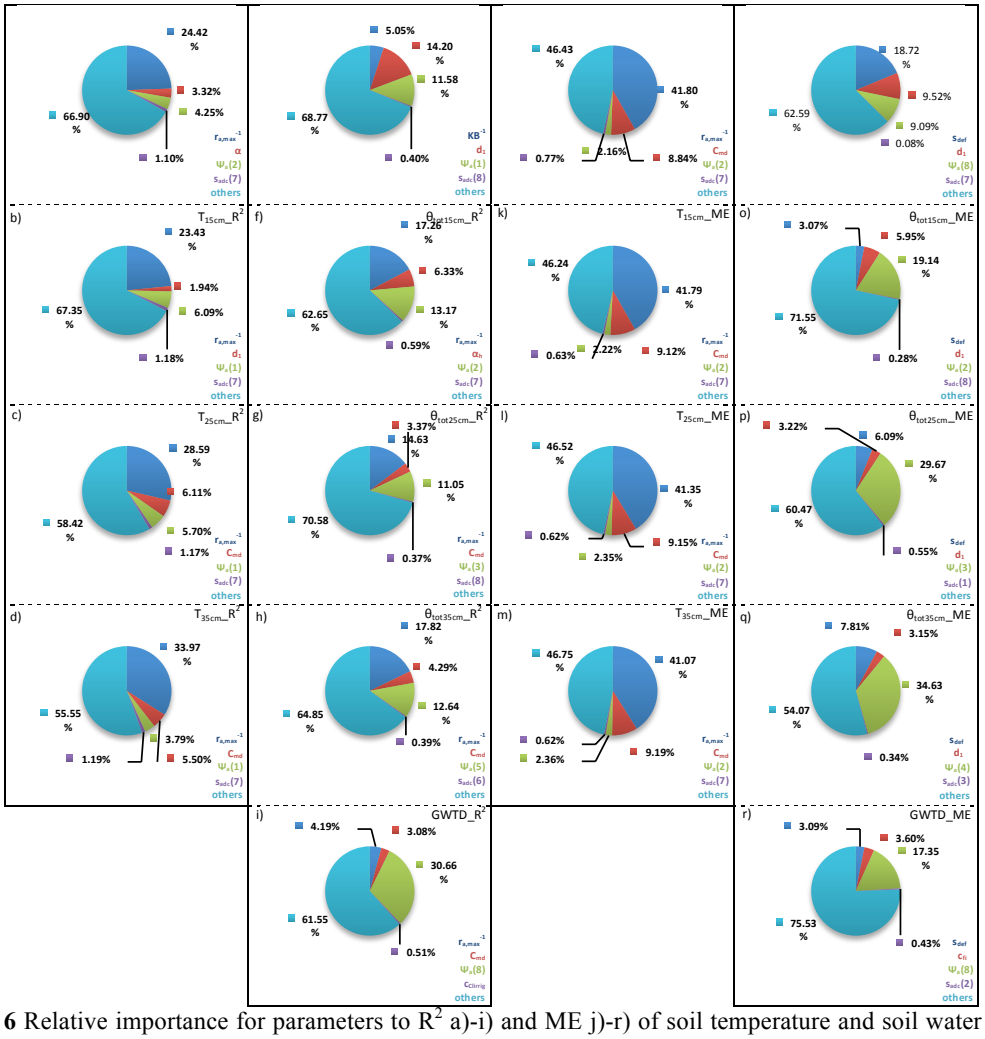

Fig. 6 Relative importance for parameters to R^2 a)-i) and ME j)-r) of soil temperature and soil water at 4 depths (5, 15, 25, 35 cm) as well as groundwater at site Yonglian. Parameters shown in each sub-figure are the most important parameter from each group, i.e. energy balance, soil heat, soil water, soil salt, then the other parameters.

At site Yonglian, $r_{a,max}^{-1}$ is shown to be the most important parameter to soil temperature R^2 at 4 depths (**Fig. 6** a)-d)). The other important parameters were related to soil frost and soil water characteristics (e.g. α, d_1, C_{md}, ψ_a). For soil total water content and groundwater table depth R^2, the important parameters from different groups were also important to soil temperature R^2. We can see that except for ψ_a at various

438 depths, the most important parameters were related to energy balance and soil heat transport in frozen
439 soils (e.g. kB^{-1}, $r_{a,max}^{-1}$, d_1, C_{md}, α_h) (**Fig 6** e)-i)). For soil temperature ME (**Fig. 6** j)-m)), the same
440 parameters were shown important as soil temperature R^2. For soil total water content and groundwater
441 table depth ME (**Fig. 6** n)-r)), the most important parameters were s_{def}, d_1 and ψ_a from different soil
442 depths. s_{def} is the maximum soil surface water deficit for calculation of surface water balance and
443 adjusting soil surface vapour pressure. It determines the estimate of soil evaporation. The great
444 importance of s_{def} to soil water ME indicated that at site Yonglian, soil evaporation is important in soil
445 water transport.

446 Soil salt related parameters did not show that great importance (around 1% relative importance) to soil
447 temperature and soil water at two sites. Even we have developed a new relationship between osmotic
448 potential and soil freezing temperature and it has shown to be able to improve model performance on
449 simulation of soil temperature, the parameter sc did not show great importance at two sites. This
450 indicated that for two sites, sc could be assigned as fixed values for different types of salt. We only
451 noticed the adsorption coefficients of salt at various layers show some importance to soil temperature and
452 water. This was because they determine the osmotic potential of soil water and thus impact soil heat and
453 water transport simulation.

454 *4.3 Prior and posterior parameters*

455 In **Table 3**, the important parameters and their posterior ranges at two sites are depicted. The posterior
456 mean value of $r_{a,max}^{-1}$ was reduced to 1/3 of prior mean value, and mean value for d_1 was also reduced
457 from prior at site Qianguo. The R_{ratio} (range ratio, defined as the posterior range width ratio to prior range
458 width) for $r_{a,max}^{-1}$ and d_1 was 0.12 and 0.18, respectively for site Yonglian (**Table 3**). Parameters
459 $z_{0M,snow}$, a_{scale} and C_{md} at site Yonglian had larger posterior mean values than prior, and the R_{ratio} was
460 0.54 and 0.68, respectively. Parameters $\psi_a(1)$ to $\psi_a(3)$ at site Yonglian also obtained generally larger
461 posterior mean values after calibration, with R_{ratio} of 0.18 to 0.50.

Hydrol. Earth Syst. Sci. Discuss., https://doi.org/10.5194/hess-2018-466
Manuscript under review for journal Hydrol. Earth Syst. Sci.
Discussion started: 8 October 2018

Hydrology and Earth System Sciences
Discussions

462 **Table 3** Important parameters and their accepted ranges at site Qianguo and Yonglian.

Parameters	Explanation	Posterior values		Accepted runs mean	[a]R_{ratio}
		Minimum	Maximum		
$r_{a,max}^{-1}$	Minimum turbulent exchange coefficient for bare soil in **Equation (A18)** (Jordan, 1991)	[b]0.51(0.01)	0.57(0.04)	0.54(0.02)	0.12(0.58)
d_1	Fraction of unfrozen water to wilting point when soil temperature is at -5 °C in **Equation (16)**	0.40(0.23)	0.48(0.45)	0.43(0.34)	0.18(0.39)
C_{md}	Maximum frozen soil thermal conductivity damping coefficient in **Equation (A12)**	0.67(0.80)	0.87(0.89)	0.76(0.86)	0.52(0.22)
$z_{0M,snow}$	Momentum roughness length of snow (m) in **Equation (A16)**	0.02	0.04	0.03	0.54
a_{scale}	Matric water adsorption coefficient for calculation of s_{mat} in **Equation (A2)**	2.78	9.55	6.36	0.68
$s_{adc}(1)$	Adsorption coefficient of salt in **Equation (11)**	(0.04)	(0.50)	(0.24)	(0.93)
$s_{adc}(2)$	Adsorption coefficient of salt in **Equation (11)**	(0.02)	(0.49)	(0.21)	(0.91)
$s_{adc}(3)$	Adsorption coefficient of salt in **Equation (4)**	(0.10)	(0.50)	(0.33)	(0.74)
$s_{adc}(4)$	Adsorption coefficient of salt in **Equation (4)**	(0.01)	(0.48)	(0.24)	(0.76)
$\psi_a(1)$	Air entry value of soil (%) in Brooks & Corey equation in **Equation (A3)**	38.34(30.94)	89.91(97.24)	57.71(65.12)	0.46(0.81)
$\psi_a(2)$	Air entry value of soil (%) in Brooks & Corey equation in **Equation (A3)**	26.49(15.94)	97.00(93.72)	80.36(48.49)	0.18(0.78)
$\psi_a(3)$	Air entry value of soil (%) in Brooks & Corey equation in **Equation (A3)**	40.83(30.60)	92.27(99.02)	68.83(64.46)	0.50(0.66)
$\psi_a(4)$	Air entry value of soil (%) in Brooks & Corey equation in **Equation (A3)**	(27.33)	(63.93)	(41.18)	(0.36)

463 [a]Rratio ratio of posterior parameter range to prior parameter range
464 [b]value without brackets is for site Qianguo, value with brackets is for site Yonglian
465

466 For C_{md} at site Yonglian, the R_{ratio} was 0.22, much smaller than at site Qianguo (0.52). R_{ratio} of d_1 at
467 site Yonglian was 0.39, larger than at site Qianguo (0.18). Parameter $r_{a,max}^{-1}$ at site Yonglian showed
468 totally different R_{ratio} and posterior mean values from site Qianguo, with R_{ratio} of 0.58 and posterior mean
469 value of 0.02, respectively. As discussed above, C_{md}, d_1 and $r_{a,max}^{-1}$ were important parameters at both
470 sites. They controlled soil heat and energy balance and can influence soil freezing/thawing. Salt
471 adsorption coefficient s_{adc} at four depths did not show large changes between posterior and prior

distributions, with R_{ratio} from 0.74 to 0.93. The R_{ratio} of ψ_a from four depths at site Yonglian varied from 0.36 to 0.81. The large differences in posterior ranges of these parameters indicated these two sites have different surface water and energy balance situations. Site Qianguo is more humid in winter and has more snow events, while site Yonglian has very dry winter but more salt influences on freezing/thawing due to higher salinity at this site. At site Qianguo, parameters such as $z_{0M,snow}$ and a_{scale} also showed to be important, and s_{adc} at various depths at site Yonglian were shown to be very sensitive.

4.4 Soil temperature and water

At site Qianguo, soil temperature and soil liquid water content were measured manually at daily resolution due to difficulties in installing automatic measurement instruments at farmers' land. Accepted simulations generally can capture soil temperature and water dynamics and can cover the observations within their ranges (**Fig. 7** a)-b)). After calibration, the mean value of R^2 for soil temperature and soil liquid water content at 5 cm depth was 0.87 and 0.31, respectively. Meanwhile, the mean values of ME for soil temperature and soil liquid water content at 5 cm depth was -0.41 ^{o}C and -4.89%, respectively.

At site Yonglian, hourly soil temperature was obtained in calibration, and achieved high R^2 for soil temperature, with mean R^2 of 0.90 at 5 cm depth. However, soil temperature was underestimated from end of November to middle of January (**Fig. 7** c)). This was mainly due to ice coverage at site Yonglian during this period. After flooding irrigation at the beginning of November, water ponding in the field (~10 cm water) was rapidly frozen and kept covering soil surface until middle of January. For this period, ice coverage disturbed water and energy balance at the site Yonglian. Even the snowpack was considered at site Yonglian and a detailed scheme for snow water and energy balance was illustrated in CoupModel, it obviously cannot describe ice coverage in our case. In the future development of the CoupModel, we recommended inclusion of a new scheme for water and energy balance on ice coverage.

Hydrol. Earth Syst. Sci. Discuss., https://doi.org/10.5194/hess-2018-466
Manuscript under review for journal Hydrol. Earth Syst. Sci.
Discussion started: 8 October 2018

Hydrology and Earth System Sciences
Discussions

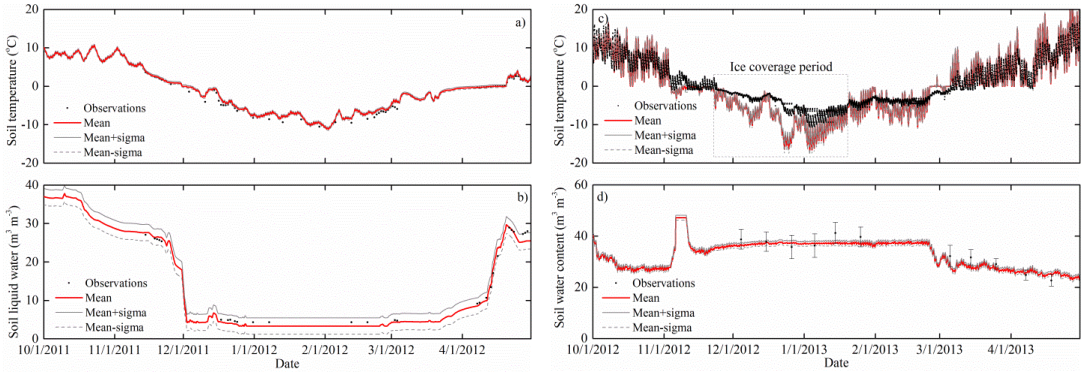

494 **Fig. 7** Comparison of soil temperature and soil water at 5 cm depth at two sites. a)-b) at site Qianguo, c)-d)
495 at site Yonglian. Red line for mean of behavioral simulations, grey lines for simulated mean values +/-
496 standard deviation (sigma), error bar in d) for standard deviation of observations from various plots.

497 Due to failure of TDR in measuring water in salinized frozen soil, we only sampled total water content
498 at site Yonglian. Soil total water content at 5 cm depth had good performance with mean R^2 from
499 accepted simulations of 0.80. Even with only 14 sampling dates from each of five plots were selected, the
500 calibrated model can capture soil water dynamics well. Nevertheless, we also noticed large variations in
501 measured total water content from different plots, as indicated by error bars in **Fig. 7** d). In the future
502 development of soil water measurement methods, it is necessary to introduce more accurate measurement
503 methods for soil water in saline frozen soils in order to obtain consistent observations of soil water
504 dynamics during winter.

505 *4.5 Model validation on water and salt storage*

506 Comparison of simulated water storage with measured water storage at different soil depths is depicted
507 in **Fig. 8**. Results indicated that CoupModel could predict water process well in upper 40 cm soil layer,
508 but some large deviations mainly occurred for 40 to 100 cm at two sites between simulated and observed
509 soil water storages. This was because the accepted simulations was derived by constraining model
510 performance for variables (soil temperature and soil water) in upper 40 cm soil layer, and the data from
511 40-100 cm depth was not used for calibration. This indicated that there might be some unforeseen

Hydrol. Earth Syst. Sci. Discuss., https://doi.org/10.5194/hess-2018-466
Manuscript under review for journal Hydrol. Earth Syst. Sci.
Discussion started: 8 October 2018

Hydrology and Earth System Sciences
Discussions

512 processes in the lower soil layer, and they would influence water processes in whole soil profile (from
513 surface to groundwater). Since the calibration was focusing on the surface water and energy balance, and
514 the upper layer water process was shown to be well-represented by the model, the more detailed
515 consideration of lower layer water processes exceeded the scope of this study. Further work would
516 include calibration of the model in the whole soil profile with more detailed measurements.

517 **Fig. 9** shows the simulated salt storage in comparison with measured salt storage based on measured
518 data at various soil depths. At site Qianguo, the Br^- storage was generally overestimated by the model in
519 comparison with measured Br^- storage in whole soil profile. The simulated Br^- storage showed larger
520 uncertainty than the measured. Similarly, at site Yonglian, the simulated Cl^- storage at various layers was
521 larger than measured Cl^- storage.

522

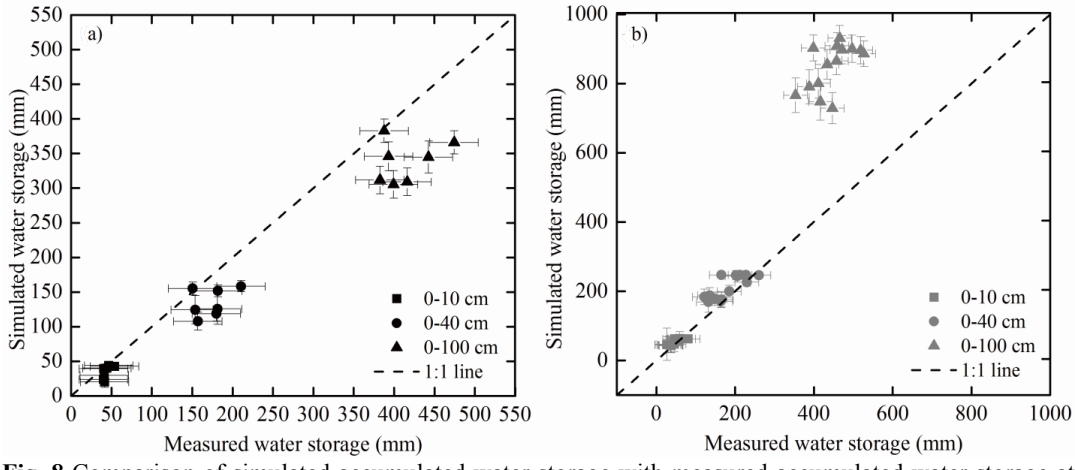

523 **Fig. 8** Comparison of simulated accumulated water storage with measured accumulated water storage at
524 two sites at various soil depths. a) site Qianguo and b) site Yonglian. X error bar denotes standard
525 deviation of observations from various plots, Y error bar denotes standard deviation of water storage from
526 behavioral simulations.

Hydrol. Earth Syst. Sci. Discuss., https://doi.org/10.5194/hess-2018-466
Manuscript under review for journal Hydrol. Earth Syst. Sci.
Discussion started: 8 October 2018

527 The overestimation of Cl^-/Br^- storage at various depths indicated that the upward movement of salt
528 with water was over-estimated. This might be due to the neglecting of diffusion and expulsion of salt in
529 model. Cary and Mayland (1972) have shown that, the diffusion and expulsion processes in frozen soil
530 actually played important roles in salt transport even though the convection was the major process. This
531 was because when soil was frozen, soil solution concentrated. The concentration of soil solution would
532 increase salt concentration gradient between soil layers. In addition, high salt concentration at low
533 temperature would cause salt expulsion from solution due to low salt saturation (Wang et al., 2016).
534 However, it was difficult to measure the diffusion and expulsion of salt in frozen soil. More detailed
535 experiments on diffusion and expulsion of salt are necessary in study of water, heat and salt coupled
536 transport in frozen soils. Validation of soil water and salt storage more data on salt transport as well as
537 water transport would be of importance in calibration of model, since the water and salt transport
538 processes are tightly coupled.

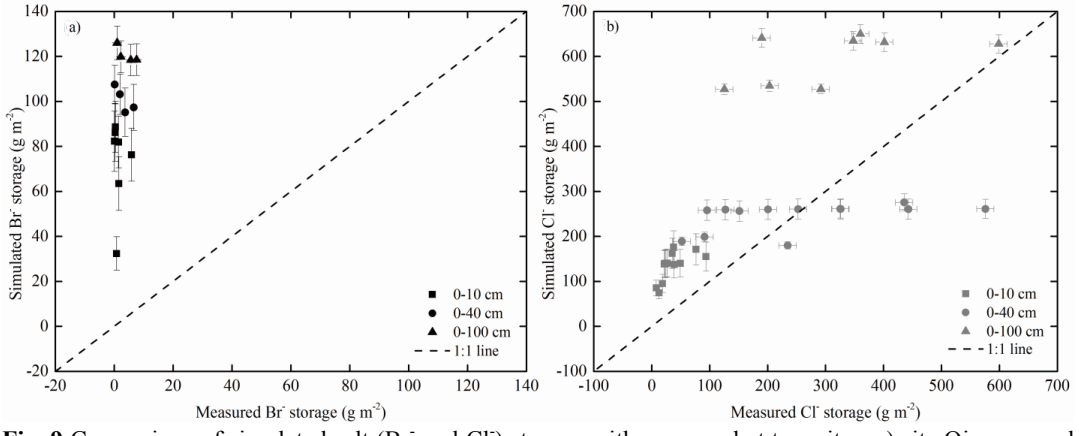

539 **Fig. 9** Comparison of simulated salt (Br^- and Cl^-) storage with measured at two sites. a) site Qianguo and
540 b) site Yonglian. X error bar denotes standard deviation of observations from various plots, Y error bar
541 denotes standard deviation of salt storage from behavioral simulations.

542 **5. Conclusions**

Water, heat and salt migrations are coupled in agricultural field. It is important to understand the mechanisms behind this coupling for better water management in cold arid regions. In this study, water, temperature and salt transport during freezing/thawing was simulated and compared with measurements in two seasonally frozen soils in northern China. Uncertainties in both measurements and model were evaluated using Monte-Carlo sampling method and a newly developed CoupModel including salt influences on soil freezing point. Multiple criteria were applied to different model performance metrics for selection of behavioral simulations in evaluating soil temperature, liquid or total water content and groundwater table. With the new freezing point determination methods, simulated soil temperature performance was improved with respect to mean error (ME), by 16% to 77%. Parameters determining energy balance at soil surface as well as soil freezing characteristics were shown important for modeling soil water and heat transport processes in LGM analysis. Parameters such as $r_{a,max}^{-1}$, d_1 and C_{md} had large differences in posterior distributions from prior distributions, with posterior range ratio (R_{ratio}) of 0.12 to 0.52 and 0.22 to 0.58 at site Qianguo and site Yonglian, respectively. Calibration of the important parameters has improved model performance a lot, with mean posterior R^2 values for soil temperature of 0.87 and 0.90, and mean posterior R^2 values for soil water (liquid and total) of 0.31 and 0.80, at site Qianguo and Yonglian, respectively. Validating of the calibrated model results against soil water and salt storages at different depths has shown that soil water storage was well represented at upper soil layers form surface to 40 cm depth, with water storage at 40-100 cm depth at site Qianguo underestimated, and water storage at 40-100 cm depth overestimated. Meanwhile, salt storage at two sites were generally overestimated by the model in the whole 0-100 cm soil profile, mainly due to lack in considering more salt transport processes such as diffusion and expulsion in frozen soils. The study has emphasized that taking influences of salt on freezing point depression into account in CoupModel can improve model performance and reduce modeling uncertainty. But detailed experiments and model development on salt transport mechanism (e.g. diffusion and expulsion of salt in frozen soils) would be very necessary in investigation of salinization and in water management in cold arid agricultural regions.

Acknowledgements

This research was funded by the National Key Research and Development Program of China (Grant Nos. 2017YFC0403304, 2016YFC0501304, 2016YFC0400203), Major Program of National Natural Science Foundation of China (Grant Nos. 51790532, 51790533) and Open Foundation of State Key Laboratory of Water Resources and Hydropower Engineering Science (No. 2017NSG02). We would like to thank Ms. Ai'ping Chen and Mr. Yang Xu from the Yichang Experimental Site for supplying the meteorological data of the studied sites. The authors also appreciate Mr. Pengju Yang, Mr. Dacheng Li and Mr. Weixing Quan for helping analyze the soil samples and processing data in laboratory.

References

Andersland, O.B., Wiggert, D.C. and Davies, S.H.: Frozen soil subsurface barriers: Formation and ice erosion, Journal of contaminant hydrology, 23, 133-147, 1996.

Azmatch, T.F., Sego, D.C., Arenson, L.U. and Biggar, K.W.: Using soil freezing characteristic curve to estimate the hydraulic conductivity function of partially frozen soils, Cold Regions Science and Technology, 83-84, 103-109, 2012.

Baker, G. and Osterkamp, T.: Salt redistribution during freezing of saline sand columns at constant rates, Water Resources Research, 25, 1825-1831, 1989.

Baker, J.M. and Spaans, E.J.A.: Mechanics of meltwater movement above and within frozen soil, International Symposium on Physics, Chemistry, and Ecology of Seasonally Frozen Soils, 97, 31-36, 1997.

Balland, V. and Arp, P.A.: Modeling soil thermal conductivities over a wide range of conditions, Journal of Environmental Engineering and Science, 4, 549-558, 2005.

Banin, A. and Anderson, D.M.: Effects of salt concentration changes during freezing on the unfrozen water content of porous materials, Water Resour. Res., 10, 124-128, 1974.

Beven, K.: A manifesto for the equifinality thesis, Journal of hydrology, 320, 18-36, 2006.

Beven, K. and Binley, A.: The future of distributed models: model calibration and uncertainty prediction, Hydrological processes, 6, 279-298, 1992.

Black, P.B. and Tice, A.R.: Comparison of soil freezing curve and soil-water curve for Windsor sandy loam, Water Resour. Res., 25, 2205-2210, 1989.

Brooks, R.H. and Corey, A.T.: Hydraulic properties of porous media and their relation to drainage design, Transactions of the ASAE, 7, 26-28, 1964.

Cary, J. and Mayland, H.: Salt and water movement in unsaturated frozen soil, Soil Science Society of America Journal, 36, 549-555, 1972.

Cary, J.W., Papendick, R.I. and Campbell, G.S.: Water and salt movement in unsaturated frozen soil: Principles and field observations, Soil Sci. Soc. Am. J., 43, 3-8, 1979.

Fuchs, M., Campbell, G. and Papendick, R.: An analysis of sensible and latent heat flow in a partially frozen unsaturated soil, Soil Science Society of America Journal, 42, 379-385, 1978.

Gustafsson, D., Lewan, E. and Jansson, P.-E.: Modeling water and heat balance of the boreal landscape-comparison of forest and arable land in Scandinavia, Journal of applied meteorology, 43, 1750-1767, 2004.

607 Gustafsson, D., Stähli, M. and Jansson, P.-E.: The surface energy balance of a snow cover: comparing
608 measurements to two differentsimulation models, Theoretical and Applied Climatology, 70, 81-
609 96, 2001.
610 Hansson, K., Simunek, J., Mizoguchi, M. and Genuchten, M.T.v.: Water flow and heat transport in frozen
611 soil: Numerical solution and freeze-thaw applications, Vadose Zone Journal, 3, 693-704, 2004.
612 Hayashi, M., Quinton, W.L., Pietroniro, A. and Gibson, J.J.: Hydrologic functions of wetlands in a
613 discontinuous permafrost basin indicated by isotopic and chemical signatures, Journal of
614 Hydrology, 296, 81-97, 10.1016/j.jhydrol.2004.03.020, 2004.
615 Jansson, P.-E.: CoupModel: model use, calibration, and validation, Transactions of the ASABE, 55, 1337-
616 1344, 2012.
617 Jansson, P.-E. and Karlberg, L.: CoupModel: Coupled heat and mass transfer model for soil-plant-
618 atmosphere systems, TRITA-LWR Report 3087. Stockholm, Sweden: Royal Institute of
619 Technology, Department of Land and Water Resources Engineering.2004.
620 Jones, J.S.: State-of-the-art report—Engineering practice in artificial ground freezing, Engineering
621 Geology, 18, 313-326, 1981.
622 Jordan, R.: A one-dimensional temperature model for a snow cover: Technical documentation for
623 SNTHERM. 89, 1991.
624 Khoshkhoo, Y., Jansson, P.E., Irannejad, P., Khalili, A. and Rahimi, H.: Calibration of an energy balance
625 model to simulate wintertime soil temperature, soil frost depth, and snow depth for a 14year
626 period in a highland area of Iran, Cold Regions Science and Technology, 119, 47-60, 2015.
627 Konrad, J.-M. and McCammon, A.: Solute partitioning in freezing soils, Canadian Geotechnical Journal,
628 27, 726-736, 1990.
629 Li, R., Shi, H., Flerchinger, G., Akae, T. and Wang, C.: Simulation of freezing and thawing soils in inner
630 Mongolia Hetao Irrigation District, China, Geoderma, 173, 28-33, 2012.
631 Lindeman, R., Merenda, P. and Gold, R.: Introduction to Bivariate and Multivariate Analysis (London,
632 Foresman and Co.), 1980.
633 Liu, H.-q., Xu, J.-w. and Wu, X.-q.: Present situation and tendency of saline-alkali soil in west Jilin
634 Province, Journal of Geographical Sciences, 11, 321, 2001.
635 Lopez, C., Brouchkov, A., Nakayama, H., Takakai, F., Fedorov, A. and Fukuda, M.: Epigenetic salt
636 accumulation and water movement in the active layer of central Yakutia in eastern Siberia,
637 Hydrological Processes, 21, 103-109, 2007.
638 McCauley, C.A., White, D.M., Lilly, M.R. and Nyman, D.M.: A comparison of hydraulic conductivities,
639 permeabilities and infiltration rates in frozen and unfrozen soils, Cold Regions Science and
640 Technology, 34, 117-125, 2002.
641 Metzger, C., Jansson, P.-E., Lohila, A., Aurela, M., Eickenscheidt, T., Belelli-Marchesini, L., Dinsmore,
642 K., Drewer, J., van Huissteden, J. and Drösler, M.: CO_2 fluxes and ecosystem dynamics at five
643 European treeless peatlands–merging data and process oriented modeling, Biogeosciences, 12,
644 125-146, 2015.
645 Mualem, Y.: A new model for predicting the hydraulic conductivity of unsaturated porous media, Water
646 resources research, 12, 513-522, 1976.
647 Okkonen, J. and Kløve, B.: A sequential modelling approach to assess groundwater–surface water
648 resources in a snow dominated region of Finland, Journal of hydrology, 411, 91-107, 2011.
649 Scherler, M., Hauck, C., Hoelzle, M. and Salzmann, N.: Modeled sensitivity of two alpine permafrost
650 sites to RCM ‐ based climate scenarios, Journal of Geophysical Research: Earth Surface, 118,
651 780-794, 2013.
652 Seyfried, M. and Murdock, M.: Use of air permeability to estimate infiltrability of frozen soil, Journal of
653 Hydrology, 202, 95-107, 1997.
654 Spaans, E.J.A. and Baker, J.M.: The soil freezing characteristic: Its measurement and similarity to the soil
655 moisture characteristic, Soil Science Society of America Journal, 60, 205-210, 1996.
656 Stähli, M., Jansson, P.E. and Lundin, L.C.: Preferential water flow in a frozen soil-A two-domain model
657 approach, Hydrological processes, 10, 1305-1316, 1996.

Wang, K., Wu, M. and Zhang, R.: Water and Solute Fluxes in Soils Undergoing Freezing and Thawing, Soil Science, 181, 193-201, 2016.

Watanabe, K., Kito, T., Dun, S., Wu, J.Q., Greer, R.C. and Flury, M.: Water Infiltration into a Frozen Soil with Simultaneous Melting of the Frozen Layer, Vadose Zone Journal, 12, 0, 10.2136/vzj2011.0188, 2013.

Wettlaufer, J. and Worster, M.G.: Premelting dynamics, Annu. Rev. Fluid Mech., 38, 427-452, 2006.

Williams, P.J.: Unfrozen water content of frozen soils and soil moisture suction, Géotechnique, 14, 231-246, 1964.

Wu, J., Jansson, P.E., van der Linden, L., Pilegaard, K., Beier, C. and Ibrom, A.: Modelling the decadal trend of ecosystem carbon fluxes demonstrates the important role of functional changes in a temperate deciduous forest, Ecological Modelling, 260, 50-61, 10.1016/j.ecolmodel.2013.03.015, 2013.

Wu, M., Huang, J., Wu, J., Tan, X. and Jansson, P.-E.: Experimental study on evaporation from seasonally frozen soils under various water, solute and groundwater conditions in Inner Mongolia, China, 535 http://dx.doi.org/10.1016/j.jhydrol.2016.01.050, 2016a.

Wu, M., Jansson, P.-E., Tan, X., Wu, J. and Huang, J.: Constraining parameter uncertainty in simulations of water and heat dynamics in seasonally frozen soil using limited observed data, Water, 8, 64, 2016b.

Wu, S., Jansson, P.E. and Zhang, X.: Modelling temperature, moisture and surface heat balance in bare soil under seasonal frost conditions in China, European Journal of Soil Science, 62, 780-796, 2011.

Zhang, W., Wang, G., Zhou, J., Liu, G. and Wang, Y.: Simulating the Water-Heat Processes in Permafrost Regions in the Tibetan Plateau Based on CoupModel, Journal of Glaciology and Geocryology, 34, 1099-1109, 2012.

Zhou, X., Zhou, J., Kinzelbach, W. and Stauffer, F.: Simultaneous measurement of unfrozen water content and ice content in frozen soil using gamma ray attenuation and TDR, Water Resources Research, 50, 9630-9655, 2014.

Appendix

Table A1 Calibrated parameters with their prior ranges.

Model parameters	Descriptions	Symbol	[c]Equation	Prior	
				Min	Max
Soil water processes calibrated parameters					
DvapTortuosity	Tortuosity of vapour	d_{vapb}	A1	0.01	2
AScaleSorption	Soil matric water adsorption coefficient	[a]a_{scale}	A2	0.1 /[b]0.02	10 /[b]0.1
Air Entry(1)-Air Entry(8)	Air entry value of soil (%)	ψ_a	A3	0.01	100
HighFlowDampC	Damping coefficient for hydraulic conductivity in high-flow domain (%)	$c_{\theta,i}$	A5	0.1 /[b]0.1	80 /[b]50
LowFlowCondImped	Impedance coefficient for hydraulic conductivity in low-flow domain due to ice existence	c_{fi}	A6	0.1	10
MinimumCond	Minimum hydraulic conductivity for	[a]$k_{min\ uc}$	A7	0.0001	0.001

Hydrol. Earth Syst. Sci. Discuss., https://doi.org/10.5194/hess-2018-466
Manuscript under review for journal Hydrol. Earth Syst. Sci.
Discussion started: 8 October 2018

Value	determining hydraulic conductivity change with soil temperature (mm d^{-1})			/[b]1.0E-06	/[b]1.0E-05
SurfPoolMax	Maximum soil surface pool (mm)	w_{pmax}	A8	20	100
DrainSpacing	Distance between two drainage tubes (m)	d_p	A9	250	300
DrainLevel	Initial drainage level (m)	z_p	A9	-2.5	-2
EmpGFLevPeak	Empirical groundwater level peak value (m)	z_1	A10	-1.5	-0.5
EmpGFlowPeak	Empirical groundwater flow peak value (m)	q_1	A11	5	15
InitialGroundWater	Initial groundwater table depth (m)	-	-	-1 /[b]-2.2	-0.5 /[b]-1.8
DrainLevelMin	Minimum drainage level (m)	-	-	-1.5	-0.5
Soil heat processes calibrated parameters					
Ballard_Arp Alpha	Coefficient for calculation of thermal conductivity with Ballard & Arp method	α	A11	0.1	0.3
Ballard_Arp Beta	Coefficient for calculation of thermal conductivity with Ballard & Arp method	β	A11	10	30
Ballard_Arp a	Coefficient for calculation of thermal conductivity with Ballard & Arp method	a	A11	0.4	0.6
CfrozenMaxDamp	Maximum damping coefficient of frozen soil thermal conductivity	C_{md}	A12	0.5	0.9
AlphaHeatCoef	Heat transfer coefficient for re-freezing of water in high-flow domain (W m^{-1} $^oC^{-1}$)	$^a\alpha_h$	A13	0.1 /[b]500	5000 /[b]5000
FreezepointFWi	Coefficient for determining liquid water content when soil is frozen at -5 ^oC	d_1	Equation(16)	0.1	0.5
Soil salt processes calibrated parameters					
SaltInitConc	Initial salt concentration (mg L^{-1})	$^ac_{Cl}$	-	20 /[b]800	40 /[b]1200
SaltInputConc	Salt concentration from precipitation input (mg L^{-1})	$^ac_{Cldep}$	-	1 /[b]0.01	10 /[b]500
SaltIrrigationConc	Salt concentration from irrigation (mg L^{-1})	$^ac_{Clirrig}$	-	1500 /[b]500	2500 /[b]1000
Ad_c(1)-Ad_c(16)	Salt adsorption coefficient	s_{adc}	-	0	0.5
Energy balance processes calibrated parameters					
EquilAdjustPsi	Coefficient for adjustment of vapor difference between upper soil and surface	ψ_{eg}	A14	0.5	1.2
MaxSurfExcess	Maximum soil surface water excess in surface water balance estimate (mm)	s_{excess}	A15	0.5	2
MaxSurfDeficit	Soil surface maximum water deficit in surface water balance estimate (mm)	s_{def}	A15	-3	-1
RoughLBareSoilMom	Momentum roughness length of bare soil (m)	$^aZ_{0M}$	A16	1.0E-05	0.05
RoughLMomSnow	Momentum roughness length of snow	$^az_{0M,snow}$	A16	0.005 /[b]0.025	0.05 /[b]0.05
KBMinusOne	Ratio of momentum and heat roughness length	kB^{-1}	A17	0	2.5
WindLessExchangeSoil	Windless exchange coefficient of bare soil	$r_{a,max}^{-1}$	A18	0.5 /[b]1.0E-04	1 /[b]0.05
MaxSoilCondens	Maximum soil water condensation rate (mm d^{-1})	$e_{max,cond}$	A19	2/[b]1	4/[b]2
KonzelmannCoef_1	Konzelmann coefficient for estimate of longwave radiation	r_{k1}	A20	0.15	0.31
SThermalCond	Snow thermal conductivity coefficient (W	^as_k	A21	2.5E-06	1.0E-05

Hydrol. Earth Syst. Sci. Discuss., https://doi.org/10.5194/hess-2018-466
Manuscript under review for journal Hydrol. Earth Syst. Sci.
Discussion started: 8 October 2018

Coef	$m^5\ ^oC^{-1}\ kg^{-2}$)			/[b]1.0E-06	/[b]1.0E-05
AlbedoKExp	Exponential coefficient for estimate of soil albedo	k_a	A22	0.5	1.5
AlbSnowMin	Minimum snow albedo	a_{min}	A23	30	50

[a]This parameter was sampled using stochastic log distribution, the others using stochastic linear distribution
[b]Range specific for site Yonglian
[c]Equation is corresponded to the number in **Table A2** or in main text

Table A2 Calibrated parameters related equations and their descriptions in CoupModel.

Equation no.	Equations	Descriptions
	Soil water processes	
A1	$D_v = d_{\text{vapb}} f_a D_0$ $D_0 = \left(\frac{T+273.15}{273.15}\right)^{1.75}$ $c_v = \frac{M_{water} e_v}{R(T+273.15)}$ $e_v = e_s e^{\left(\frac{-\psi M_{water} e_v}{R(T+273.15)}\right)}$ where f_a is the fraction of air-filled pores, D_0 is the diffusion coefficient in free air ($m^2\ s^{-1}$) and d_{vapb} is a parameter accounting for tortuosity and the enhancement of vapor transfer observed in measurements compared with theory, ψ is matric potential (m, with positive value), M_{water} is mole mass of water (18 g mol^{-1}), R is gas constant, e_s is saturated vapor pressure (m), T is soil temperature (K).	Soil vapor diffusion coefficient
A2	$S_{\text{mat}} = a_{\text{scale}} a_{\text{r}} k_{\text{mat}}\text{pF}$ where k_{mat} is matric hydraulic conductivity (m s^{-1}), a_{r} is the ratio between compartment thickness, Δz, and the unit horizontal area represented by the model, pF is $\log_{10}\psi$, a_{scale} is an empirical scaling coefficient accounting for the geometry of aggregates.	Sorption capacity rate estimation
A3	$S_e = \left(\frac{\psi}{\psi_a}\right)^{-\lambda}$ where ψ_a is the air-entry tension (m), λ is the pore size distribution index and S_e the effective saturation.	Water retention curve defined by Brooks and Corey (1964)
A4	$k_w^* = k_{mat} S_e^{(n+2+2/\lambda)}$ wherek_{mat} is matric hydraulic conductivity (m s^{-1}), λ is the pore size distribution index, S_e the effective saturation and n is tortuosity.	Unsaturated soil hydraulic conductivity calculated by Mualem (1976) equation
A5	$k_{f\!h} = e^{-\frac{\theta_i}{c_{\theta,i}}}\left(k_w(\theta_{tot}) - k_w\left(\theta_{lf} + \theta_i\right)\right)$ where $k_w(\theta_{tot})$ is hydraulic conductivity for pores saturated with water (m s^{-1}), $k_w\left(\theta_{lf} + \theta_i\right)$ is hydraulic conductivity when water flow in low domain	Hydraulic conductivity in high flow domain

	with ice existence (m s^{-1}), $\theta_i / c_{\theta,i}$ is reduced factor, and $c_{\theta,i}$ is impedance factor.	
A6	$k_{wf} = 10^{-c_{fi}Q} k_w$ where c_{fi} is impedance factor, and Q is heat quality, as a ratio of ice content to total water content.	Hydraulic modification for low flow domain
A7	$k_w = (r_{\mathrm{AOT}} + r_{\mathrm{A1T}} T_s) \max(k_w^*, k_{\mathrm{minuc}})$ where r_{AOT}, r_{A1T} ($^{\circ}C^{-1}$) and k_{minuc} (m s^{-1}) are parameters. k_w^* is the total hydraulic conductivity (m s^{-1}), as a sum of hydraulic conductivity from matrix and macro pores.	Actual unsaturated hydraulic conductivity after temperature correction
A8	$q_{\mathrm{surf}} = a_{\mathrm{surf}} \left(W_{\mathrm{pool}} - w_{\mathrm{pmax}} \right)$ where a_{surf} is an empirical coefficient, W_{pool} is the total amount of water in the surface pool (m), and w_{pmax} is the maximal amount of water stored on soil surface without causing surface runoff (m).	Surface runoff estimation
A9	$q_{wp} = \frac{4k_{s1}(z_{sat} - z_p)}{d_p^2} + \frac{8k_{s2} z_D (z_{sat} - z_p)}{d_p^2}$ where k_{s1}, k_{s2} are saturated hydraulic conductivities above and below water level (m s^{-1}), respectively; z_D is soil depth below drainage level (m), z_p is drainage depth to soil surface (m), d_p is distance between two drainage tubes.	Hooghoudt drainage equation
A10	$q_{gr} = q_1 \frac{\max(0, z_1 - z_{sat})}{z_1} + q_2 \frac{\max(0, z_2 - z_{sat})}{z_2}$ where q_1, q_2 are maximum and minimum empirical groundwater flow (m s^{-1}), respectively; z_1 and z_2 are highest and lowest empirical groundwater level (m), respectively.	Empirical drainage equation
Soil heat processes		
A11	$K_{soil} = (K_{sat} - K_{dry}) Ke + K_{dry}$ $K_{dry} = \frac{(aK_{solid} - K_{air})\rho_b + K_{air}\rho_p}{\rho_p - (1-a)\rho_b}$ For unfrozen soils, $Ke = \theta_{sat}^{0.5\left(1+V_{om,s}-\alpha V_{sand,s}-V_{cf,s}\right)\left[\left(\frac{1}{1+\exp(-\beta\theta_{sat})}\right)^3 - \left(\frac{1-\theta_{sat}}{2}\right)^3\right]^{1-V_{om,s}}}$ For frozen or partially frozen soils, $Ke = \theta_{sat}^{1+V_{om,s}}$ where Ke is Kersten number (-), θ_{sat} is saturation (m^3 m^{-3}); $V_{om,s}$ is volumetric fraction of organic matter (-), $V_{sand,s}$ is volumetric fraction of sand (-), $V_{cf,s}$ is volumetric fraction of coarse fragments (-), α and β are adjustment factor (-), K_{solid} is solid thermal conductivity (W m^{-1} $^{\circ}C^{-1}$), K_{air} is air thermal conductivity (W m^{-1} $^{\circ}C^{-1}$), ρ_b is bulk density (kg m^{-3}), ρ_p is air density (kg m^{-3}), a is adjustment factor (-).	This is to calculate soil thermal conductivity for frozen and unfrozen conditions (Ballard and Arp, 2005)
A12	$R_f = e^{c_f T_s} C_{md} + (1 - C_{md})$ where c_f is soil surface frost adjustment coefficient ($^{\circ}C^{-1}$), C_{md} is maximum	This is used to adjustment thermal

	frost damping coefficient (-), T_s is surface soil temperature (°C)	conductivity of frozen soil
A13	$q_{\text{freeze}} = \alpha_h \Delta z \frac{T}{L_f}$ where α_h is heat transfer coefficient (W m^{-1} °C^{-1}), Δz is thickness of soil layer (m), T is soil temperature (°C), L_f is the latent heat of freezing (J m^{-3}).	Redistribution of infiltrating water from high flow to low flow domain
	Energy balance processes	
A14	$e_{\text{surf}} = e_s(T_s) e^{\left(\frac{\psi M_{\text{water}} g e_{\text{corr}}}{R(T_s+273.15)}\right)}$ $e_{\text{corr}} = 10^{\left(-\delta_{\text{surf}} \psi_{eg}\right)}$ where e_s is the vapor pressure (m) at saturation at soil surface temperature T_s (°C), ψ is the soil water tension (m) and g is the gravitational constant (g m^{-2} s^{-1}), R is the gas constant (J °C^{-1} mol^{-1}), M_{water} is the molar mass of water (18 g mol^{-1}) and e_{corr} is the empirical correction factor, ψ_{eg} is a parameter and δ_{surf} is a calculated mass balance at the soil surface (m), which is allowed to vary between the parameters s_{def} and s_{excess} given in m of water.	Vapor pressure at the soil surface
A15	$\delta_{\text{surf}}(t) = \max\left(s_{\text{def}}, \min\left(\begin{matrix} s_{\text{excess}}, \delta_{\text{surf}}(t-1) + W_{\text{pool}} + \\ \left(q_{in} - E_s - q_{v,s} + i_{\text{drip}}(z_1)\right)\Delta t \end{matrix}\right)\right)$ where W_{pool} is the surface water pool (m), q_{in} is the infiltration rate (m s^{-1}), E_s is the evaporation rate (m s^{-1}), i_{drip} is drip irrigation rate (m s^{-1}), $q_{v,s}$, is the vapor flow from soil surface to the central point of the uppermost soil layer (m s^{-1}), s_{def} is maximal surface water deficit (m) and s_{excess} is maximal surface water excess (m).	Mass balance check at the soil surface
A16	$r_{aa} = \frac{1}{k^2 u} \ln\left(\frac{z_{\text{ref}}}{z_{\text{OM}}}\right) \ln\left(\frac{z_{\text{ref}}}{z_{\text{OH}}}\right) f(R_{ib})$ where u is the wind speed (m s^{-1}) at the reference height, z_{ref} (m), R_{ib} is the bulk Richardson number, k is the von Karman constant and z_{OM} and z_{OH} are the surface roughness lengths for momentum and heat, respectively (m).	Aerodynamic resistance at stable atmosphere
A17	$kB^{-1} = \ln\left(\frac{z_{\text{OM}}}{z_{\text{OH}}}\right)$ where kB^{-1} is a parameter with a default value 0 (implies $z_{\text{OH}} = z_{\text{OM}}$).	Calculation of of z_{OH} from kB^{-1}
A18	$r_{aa} = \left(\frac{1}{r_{aa}} + r_{a,max}^{-1}\right)^{-1}$ where $r_{a,\text{max}}^{-1}$ is a parameter for a upper limit of the aerodynamic resistance in extreme stable conditions.	Aerodynamic resistance in extreme stable conditions
A19	$E_s = \max\left(-e_{\text{max,cond}}, L_v E_s / L_v\right) f_{\text{bare}}$ where $e_{\text{max,cond}}$ is maximum condensation rate (m s^{-1}) for upmost soil layer to maintain water balance, f_{bare} is bare soil fraction.	Soil evaporation limiting factor

Hydrol. Earth Syst. Sci. Discuss., https://doi.org/10.5194/hess-2018-466
Manuscript under review for journal Hydrol. Earth Syst. Sci.
Discussion started: 8 October 2018

A20	$\varepsilon_{\text{a,Konzelmann}} = \left(r_{k1} + r_{k2} \frac{e_a}{T_a + 273.15} \right)^{1/4} \left(1 - n_c^3\right) + r_{k3} n_c^3$ where e_a is vapor pressure (m), T_a is air temperature (^{o}C) n_c is cloud fraction; r_{k1}, r_{k2}, and r_{k3} are parameters.	Longwave radiation estimation
A21	$k_{\text{snow}} = s_k \rho_{\text{snow}}^2$ where s_k is empirical parameter (W m^5 ^{o}C^{-1} kg^{-2}), ρ_{snow} is density of snow (kg m^{-3}).	Thermal conductivity of snow
A22	$a_{\text{soil}} = a_{\text{dry}} + e^{-k_a^{10} \lg \psi} (a_{\text{wet}} - a_{\text{dry}})$ where a_{dry} is albedo of dry soil, a_{wet} is albedo of wet soil, and k_a is a transform coefficient from wet to dry soil.	Albedo of bare soil
A23	$a_{\text{snow}} = a_{\text{min}} + a_1 e^{a_2 S_{age} + a_3 \sum T_a}$ where a_{min} is minimum albedo of snow, S_{age} is snow age (d), a_1, a_2, and a_3 are parameter.	Albedo of snow

694

695

696